The EMBO Journal Vol. 22 No. 4 pp. 776–785, 2003

Homo- and heterotetrameric architecture of the epithelial Ca^{2+} channels TRPV5 and TRPV6

J.G.J.Hoenderop, T.Voets[1], S.Hoefs, F.Weidema, J.Prenen[1], B.Nilius[1] and R.J.M.Bindels[2]

Department of Cell Physiology, Nijmegen Centre for Molecular Life Sciences, University Medical Centre Nijmegen, PO Box 9101, NL-6500 HB Nijmegen, The Netherlands and [1]Department of Physiology, Campus Gasthuisberg, KU Leuven, Belgium

[2]Corresponding author
e-mail: r.bindels@ncmls.kun.nl

The molecular assembly of the epithelial Ca^{2+} channels (TRPV5 and TRPV6) was investigated to determine the subunit stoichiometry and composition. Immunoblot analysis of *Xenopus laevis* oocytes expressing TRPV5 and TRPV6 revealed two specific bands of 75 and 85–100 kDa, corresponding to the core and glycosylated proteins, respectively, for each channel. Subsequently, membranes of these oocytes were sedimented on sucrose gradients. Immunoblotting revealed that TRPV5 and TRPV6 complexes migrate with a mol. wt of 400 kDa, in line with a tetrameric structure. The tetrameric stoichiometry was confirmed in an electrophysiological analysis of HEK293 cells co-expressing concatemeric channels together with a TRPV5 pore mutant that reduced Cd^{2+} sensitivity and voltage-dependent gating. Immunoprecipitations using membrane fractions from oocytes co-expressing TRPV5 and TRPV6 demonstrated that both channels can form heteromeric complexes. Expression of all possible heterotetrameric TRPV5/6 complexes in HEK293 cells resulted in Ca^{2+} channels that varied with respect to Ca^{2+}-dependent inactivation, Ba^{2+} selectivity and pharmacological block. Thus, Ca^{2+}-transporting epithelia co-expressing TRPV5 and TRPV6 can generate a pleiotropic set of functional heterotetrameric channels with different Ca^{2+} transport kinetics.

Keywords: CaT1/CaT2/ECaC1/ECaC2/oligomerization

Introduction

The recent expression cloning of the epithelial Ca^{2+} channels TRPV5 and TRPV6 (originally named ECaC1 and ECaC2) has provided a molecular basis for exploring the characteristics of the rate-limiting entry step in transcellular Ca^{2+} (re)absorption (Hoenderop *et al*., 1999b; Peng *et al*., 1999; Montell *et al*., 2002). Ca^{2+}-transporting tissues, including small intestine, kidney and placenta, play a key role in calcium homeostasis of the body (Hoenderop *et al*., 2002b). At the cellular level, transcellular Ca^{2+} transport proceeds via a well controlled sequence of molecular events (Hoenderop *et al*., 2002b).

TRPV5 and TRPV6 form a distinct subfamily within the superfamily of transient receptor potential channels (TRPs). The TRP family includes a diversity of non-voltage-gated cation channels that vary significantly in their selectivity and mode of activation (Clapham *et al*., 2001; Montell *et al*., 2002). These channels fulfill important physiological functions ranging from phototransduction, olfaction, nociception, and heat and cold sensation to epithelial calcium transport (Hoenderop *et al*., 2002b). Our understanding of the function, gating, regulation and structural assembly of TRP family members is increasing rapidly. The *Drosophila* TRP and TRPL members were identified first, and it has been shown that these proteins form heteromultimeric channels associated in a supramolecular signaling complex with receptors and regulators including protein kinase C (PKC), calmodulin and the scaffolding PDZ domain-containing protein InaD (Bahner *et al*., 2000; Li and Montell, 2000). Furthermore, it has been demonstrated that TRPC1 and TRPC3 form heteromultimers with a non-selective cation permeability (Lintschinger *et al*., 2000). More recently, it has been reported that there are many channel compositions within the TRPC family, e.g. TRPC1/5 (Strubing *et al*., 2001), TRPC4/5 and TRPC3/6/7 (Strubing *et al*., 2001; Hofmann *et al*., 2002).

Detailed mRNA expression profiling demonstrated that TRPV5 and TRPV6 are co-expressed in several tissues including intestine, kidney, pancreas, prostate and testis (Muller *et al*., 2000a; Peng *et al*., 2000; Hoenderop *et al*., 2001b). Genomic analysis revealed that TRPV5 and TRPV6 originate from two genes juxtaposed on human chromosome 7q35 and mouse chromosome 6 (Muller *et al*., 2000b; Weber *et al*., 2001). These two channels share several functional properties, including the permeation profile for monovalent and divalent cations (Vennekens *et al*., 2000), anomalous mole fraction behavior (Vennekens *et al*., 2000), Ca^{2+}-dependent inactivation (Nilius *et al*., 2001a) and regulation by the calciotropic hormone 1,25-dihydroxyvitamin D_3 and Ca^{2+} itself (Hoenderop *et al*., 2001a, 2002a; van Cromphaut *et al*., 2001). However, detailed comparison of the N- and C-termini of the TRPV5 and TRPV6 channels reveals significant differences, which may account for the unique electrophysiological properties of these homologous channels (Vennekens *et al*., 2002). The initial inactivation is faster in TRPV6 than in TRPV5, and the kinetic differences between Ca^{2+} and Ba^{2+} currents are more pronounced for TRPV6 than for TRPV5 (Hoenderop *et al*., 2001b). Intriguingly, the affinity of TRPV5 for the potent channel blocker ruthenium red is 100 times higher than that of TRPV6 (Hoenderop *et al*., 2001b).

Detailed information about the composition of functional TRPV5/6 channels is a prerequisite for obtaining further insight into the molecular regulation of TRPV5 and

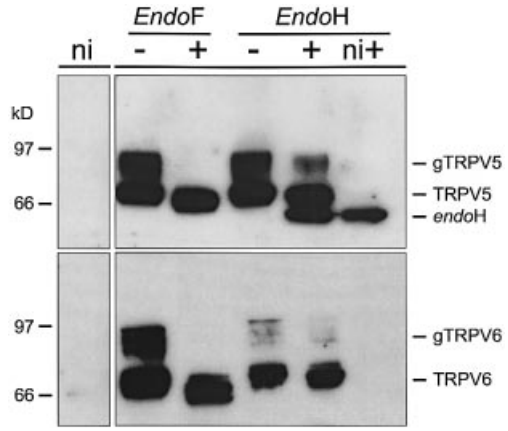

Fig. 1. Immunoprecipitation of TRPV5 (upper) and TRPV6 (lower) proteins. Membranes of non- (ni), HA-TRPV5- or Flag-TRPV6-expressing oocytes were solubilized and subjected to endoF and endoH treatment. Glycosylated TRPV5 (gTRPV5) and TRPV6 (gTRPV6) proteins are indicated, and the protein bands labeled TRPV5 or TRPV6 represent the non-glycosylated core proteins.

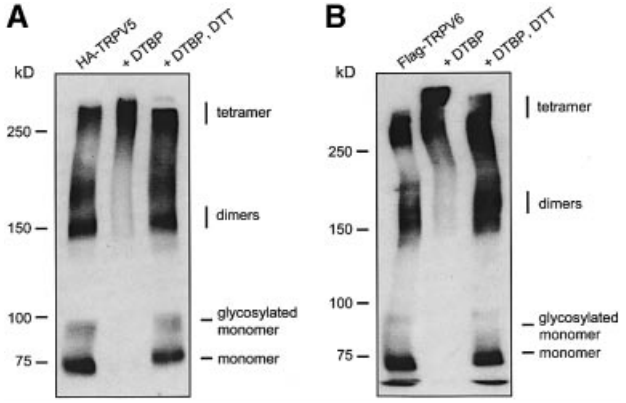

Fig. 2. Determination of the TRPV5/6 oligomeric structure using chemical cross-linking. Lysates of (**A**) TRPV5- and (**B**) TRPV6-expressing oocytes incubated with sample buffer containing DTBP. Complexes were treated with DTT and loaded in the third lane.

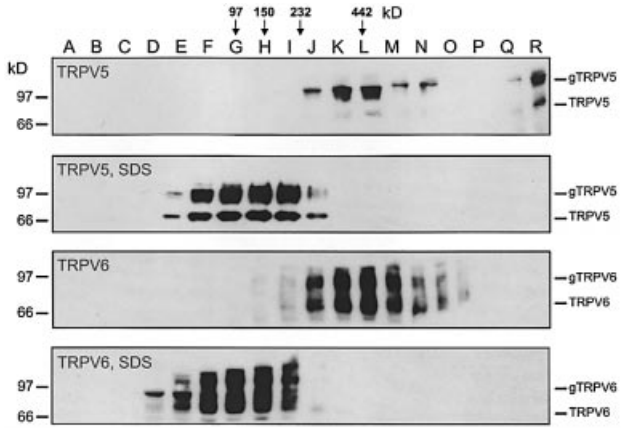

Fig. 3. Immunoblot analyses of the oligomeric state of TRPV5 and TRPV6. Membranes from TRPV5- or TRPV6-expressing oocytes were solubilized in 0.5% (w/v) deoxycholate and subjected to sucrose gradient centrifugation. SDS indicates that 0.1% (w/v) SDS has been added to the sucrose gradient. The fractions with peak intensities of the marker proteins (phosphorylase B, 97 kDa; alcohol dehydrogenase, 150 kDa; catalase, 232 kDa; apoferritin, 442 kDa) are indicated.

TRPV6. Based on the similarities in molecular structure between the members of the six transmembrane domain channel superfamily including potassium and cyclic nucleotide-gated channels, we hypothesize that active TRPV5/6 channels are composed of more than one subunit, forming homo- or heteromultimeric Ca^{2+} channels. Multimeric channels could contribute to the functional heterogeneity and complex pharmacology observed in patch–clamp experiments and Ca^{2+} uptake experiments in renal cells and different heterologous expression systems (Hoenderop *et al*., 1999b, 2002b; Nilius *et al*., 2001b).

Therefore, the aim of the present study was to evaluate the possible subunit configurations of TRPV5/6 that could provide insights into channel regulation and information facilitating the design of specific blockers. Using a combination of biochemical and electrophysiological approaches, we have demonstrated that functional TRPV5 and TRPV6 channels have a tetrameric stoichiometry. Moreover, we have shown that TRPV5 and TRPV6 are able to combine into heterotetramers with novel properties.

Results

Post-translational modification of TRPV5 and TRPV6

Heterologous expression of TRPV5 and TRPV6 in *Xenopus laevis* oocytes and subsequent immunoblot analysis of cell lysates using HA and Flag antibodies, respectively, revealed specific bands with a molecular size ranging from 75 to 85–100 kDa (Figure 1). These bands were not detected in non-injected oocytes. The immunoreactive protein bands at 75 kDa reflect the core protein, while the presence of the other TRPV5 and TRPV6 immunoreactive bands at slightly greater apparent molecular masses suggests post-translational modification. To assess this potential post-translational modification of the channel proteins, cell lysates from TRPV5- or TRPV6-expressing oocytes were incubated with endoglycosidase H (endoH), which only cleaves high mannose type sugars, or *N*-glycosidase F (endoF), which removes all types of sugars for TRPV5 and TRPV6. The 85–100 kDa bands were reduced after incubation with endoH, while the 75 kDa band remained predominant. Immunoblot analysis of HA-TRPV5 with the HA antibody resulted in an additional band at 60 kDa. This was due to immunoreactivity of endoH, as non-injected oocytes treated with this enzyme also showed this protein band (Figure 1). The disappearance of the 85–100 kDa bands upon treatment with endoF illustrates that these protein bands represent complex glycosylated TRPV5 and TRPV6.

Tetrameric stoichiometry of TRPV5 and TRPV6

To explore the oligomerization of TRPV5 and TRPV6, chemical cross-linking studies were performed using dimethyl-3,3′-dithiobispropionamidate (DTBP). Membrane preparations of TRPV5- or TRPV6-expressing oocytes were treated with DTBP and the complexes formed were

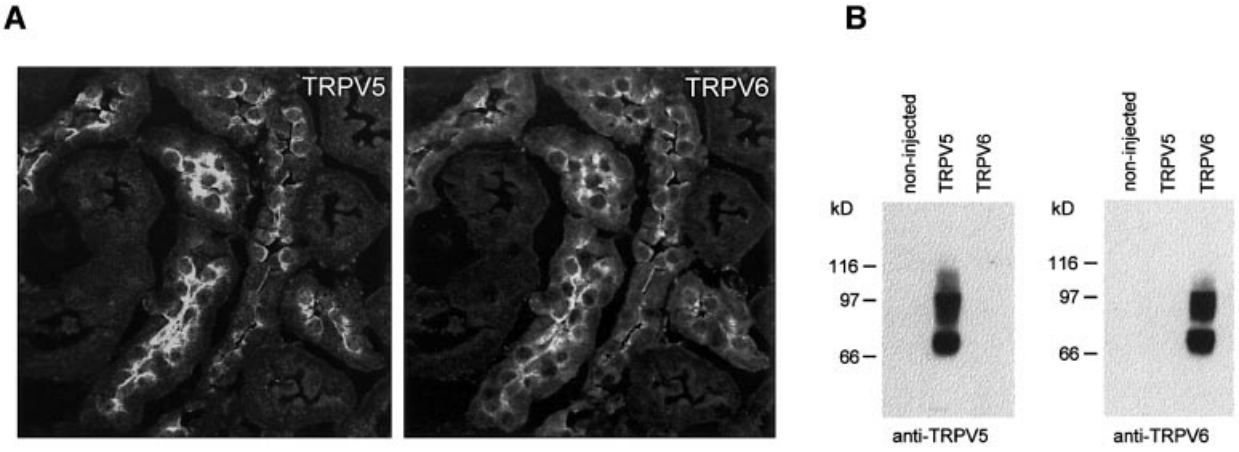

Fig. 4. Co-localization of TRPV5 and TRPV6 in kidney. (**A**) Mouse kidney cortex sections were co-stained with antibodies against TRPV5 (left) and TRPV6 (right). (**B**) Immunoblotting of membrane preparations from oocytes expressing TRPV5 and TRPV6. To exclude cross-reactivity between the antibodies, the left blot was incubated with the TRPV5 antibody and the right blot was incubated with the TRPV6 antibody.

separated on an SDS–PAGE gel and subsequently analyzed by immunoblotting. As shown in Figure 2, 75 kDa monomers of TRPV5 (Figure 2A) and TRPV6 (Figure 2B) disappeared upon treatment with DTBP, whereas the intensity of oligomeric complexes with a molecular mass >250 kDa increased concomitantly. DTBP contains a cleavable spacer, allowing the conjugate to be broken easily by dithiothreitol (DTT). Indeed, incubation of the cross-linked TRPV5 and TRPV6 complexes with DTT revealed re-occurrence of the monomers.

Since the aforementioned experiments suggest that TRPV5 and TRPV6 channels can form oligomeric complexes, we subsequently estimated the stoichiometry of the channel complexes. To this end, membranes were isolated from oocytes expressing TRPV5 or TRPV6, solubilized in 0.5% (w/v) desoxycholate and subjected to sucrose gradient centrifugation. Immunoblotting of 18 fractions (A–R) collected from the gradient revealed that the intensity of TRPV5 and TRPV6 peaked in fractions K and L (Figure 3). The sedimentation marker proteins (i.e. phosphorylase B, alcohol dehydrogenase, catalase and apoferritin), which were loaded on a parallel sucrose gradient, peaked in fractions G, H, I–J and L, respectively, as indicated by the arrows (Figure 3). A plot of the fraction with peak intensities versus the molecular mass of the marker proteins revealed that TRPV5 and TRPV6 migrate predominantly as complexes with a molecular mass of ~400 kDa, suggesting that both channels form tetrameric complexes. Sucrose gradient centrifugation in the presence of 0.1% (w/v) SDS reduced the molecular mass of TRPV5 and TRPV6 complexes to ~100 kDa (Figure 3). This treatment did not affect the distribution of the marker proteins (data not shown).

Co-localization of TRPV5 and TRPV6 in kidney

In kidney, TRPV5 is primarily expressed along the apical membrane of distal convoluted and connecting tubules (Figure 4A) (Hoenderop *et al*., 2000; Loffing *et al*., 2001). Importantly, TRPV6 was consistently detected in these TRPV5-expressing nephron segments where they both concentrated along the apical membrane of distal tubular cells. This is in line with the postulated Ca^{2+} transport function of TRPV5 and TRPV6. Expression of TRPV5 and TRPV6 in oocytes and subsequent immunoblotting demonstrated that the applied antibodies did not cross-react, indicating that both antibodies are channel specific (Figure 4B).

Co-immunoprecipitation of TRPV5 and TRPV6

The observed co-localization of the TRPV5/6 proteins in the apical membrane of distal tubular segments raises the possibility that TRPV5 and TRPV6 are able to form functional heterotetrameric ion-channel complexes. Therefore, we tested whether TRPV5 and TRPV6 can be co-immunoprecipitated from oocytes expressing both channels. First, lysates were prepared from HA-TRPV5- or Flag-TRPV6-expressing oocytes to demonstrate protein expression and specificity of the applied antibodies. Immunoblotting confirmed expression of proteins that were specifically detected by the HA and Flag antibodies, respectively (Figure 5A). Subsequently, TRPV5 and TRPV6 proteins were co-expressed and immunoprecipitated with the HA or Flag antibodies. Immunoblots containing the complexes were probed with the TRPV5 antibody or a peroxidase-coupled Flag antibody. Interestingly, the results shown in Figure 5B and C demonstrate that TRPV6 was co-immunoprecipitated with the HA TRPV5 antibody and vice versa, suggesting the existence of heteromeric TRPV5/6 channel complexes.

Functional analysis of TRPV5/6 concatemers

To corroborate the tetrameric stoichiometry of functional TRPV5/6 channels, we followed an approach similar to that used to demonstrate the subunit stoichiometry of voltage-gated K^+ channels (Liman *et al*., 1992). We constructed concatemeric cDNAs coding for 2–4 TRPV5 and/or TRPV6 monomers linked in a head-to-tail fashion. In line with the findings of Liman *et al*. (1992), we found that expression of di-, tri- and tetrameric concatemers of TRPV6 gave rise to robust whole-cell currents with properties similar to those observed upon expression of monomeric constructs (Figures 6 and 7; data not shown). Additionally, we made use of a TRPV5 pore mutant ($TRPV5^{D542A}$), which displays a strongly reduced Cd^{2+}

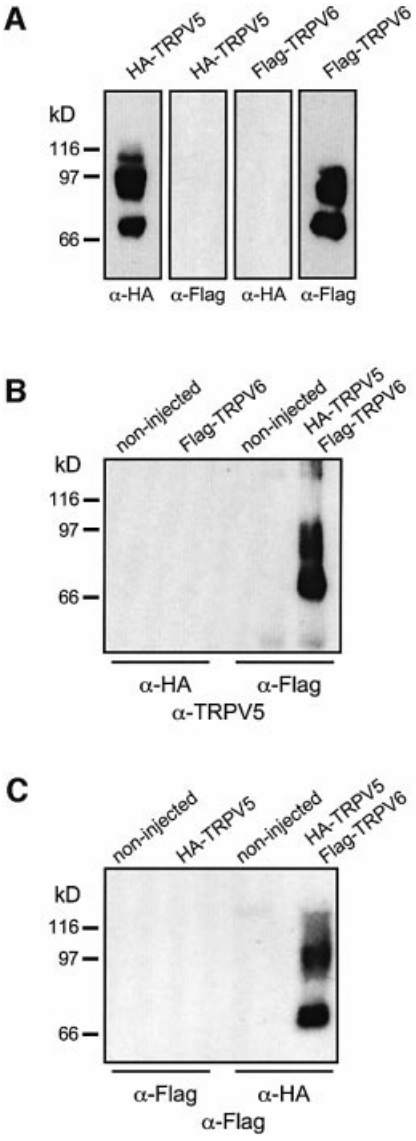

Fig. 5. Co-immunoprecipitation of TRPV5 and TRPV6. Copy RNA of HA-TRPV5 and/or Flag-TRPV6 was (co-)injected in oocytes and cell lysates were processed. (**A**) Immunoblot analysis demonstrated that both channel proteins are expressed and the applied antibodies do not cross-react. Co-immunoprecipitations were performed with the HA and Flag antibodies and subsequently immunoblots were probed using (**B**) the TRPV5 antibody and (**C**) the Flag antibody. Four oocytes expressing TRPV5 or TRPV6 were used for the immunoblot analysis depicted in (A), whereas 12 oocytes were processed for each condition in the co-immunoprecipitation experiments shown in (B) and (C). The total amount of the sample was loaded on the gel.

sensitivity compared with wild-type TRPV5 and lacks voltage-dependent gating, to probe for the incorporation of single subunits into a multimeric channel complex. Figure 6A shows current–voltage relationships for monovalent cation currents in cells expressing a tetrameric TRPV5 construct (TRPV5555) in the absence and presence of different extracellular Cd^{2+} concentrations. At –100 mV, inward currents were almost completely blocked by 2 μM Cd^{2+}. In contrast, monovalent currents in cells expressing the $TRPV5^{D542A}$ mutant were insensitive to this low Cd^{2+} concentration and were only partly blocked by concentrations up to 2 mM (Figure 6B). The dose–response curves for TRPV5555, which was not significantly different from that of monomeric TRPV5, and $TRPV5^{D542A}$ were well fitted by a simple Hill function, yielding K_D values of 64 nM and 313 μM, respectively (Figure 6G). Expression of a tetrameric TRPV5 construct in which the second repeat contains the D542A mutation ($TRPV55^{D542A}55$) led to currents with a Cd^{2+} sensitivity intermediate between those of TRPV5555 and $TRPV5^{D542A}$ (Figure 6C). The Cd^{2+} dose–response curve for $TRPV55^{D542A}55$ was well described by a single Hill function (K_D = 1.0 μM) (Figure 6H), indicating that this construct gives rise to a single population of channels different from both wild-type TRPV5 and $TRPV5^{D542A}$. The Cd^{2+} sensitivity of $TRPV55^{D542A}55$ currents also differed from that of currents obtained upon co-expression of a mixture of monomeric TRPV5 and $TRPV5^{D542A}$ in a 3:1 DNA concentration ratio (Figure 6D). The Cd^{2+} dose–response curve for this mixture could not be fitted by a single Hill function (Figure 6H), indicating that several populations of channels with distinct Cd^{2+} sensitivities are present. This is expected if the TRPV5 and $TRPV5^{D542A}$ monomers randomly combine into multimeric channels containing variable numbers of wild-type and mutant subunits. Since the Cd^{2+} sensitivity of the $TRPV55^{D542A}55$ concatemer strongly differs from that obtained for the mixture of monomeric TRPV5 and $TRPV5^{D542A}$, we can exclude the possibility that the concatemer is broken down to release individual subunits. Additionally, the finding that the $TRPV55^{D542A}55$ concatemer gave rise to a single population of channels different from both wild-type TRPV5 and $TRPV5^{D542A}$ excludes the possibility that functional channels are monomers or dimers.

Subsequently, we tested the effect of co-expression of $TRPV5^{D542A}$ together with tri- or tetrameric concatemers of TRPV6 (TRPV666 and TRPV6666) (Figure 6E and F). We argued that if functional channels were indeed tetramers, $TRPV5^{D542A}$ might be able to combine into a functional channel with the trimeric TRPV666, but not with the tetrameric TRPV6666. Currents in cells co-expressing $TRPV5^{D542A}$ and TRPV6666 consisted of a Cd^{2+}-sensitive fraction that was completely blocked at 2 μM and an insensitive fraction that was not fully blocked at 2 mM (Figure 6E). The dose–response curve for the co-expression of $TRPV5^{D542A}$ and TRPV6666 was excellently described by the weighted sum of the Hill functions for TRPV6666 and $TRPV5^{D542A}$. This result indicated that two populations of channels are present in these cells, corresponding to wild-type TRPV6 and $TRPV5^{D542A}$, respectively. Analogous results were obtained for the co-expression of TRPV5555 with $TRPV^{D542A}$ (data not shown). In contrast, the dose–response curve for the co-expression of $TRPV5^{D542A}$ and TRPV666 was less well described by such a combined function, especially at lower Cd^{2+} concentrations, indicating formation of channels that differ from both wild-type TRPV6 and $TRPV5^{D542A}$. These findings demonstrated that a trimeric concatemer is able to combine with $TRPV5^{D542A}$, whereas a tetrameric construct excludes the mutant subunit, strongly suggesting a tetrameric stoichiometry for TRPV5/6.

Additionally, we made use of the effect of the $TRPV5^{D542A}$ mutation on the voltage-dependent gating of the channel to strengthen our conclusion on the

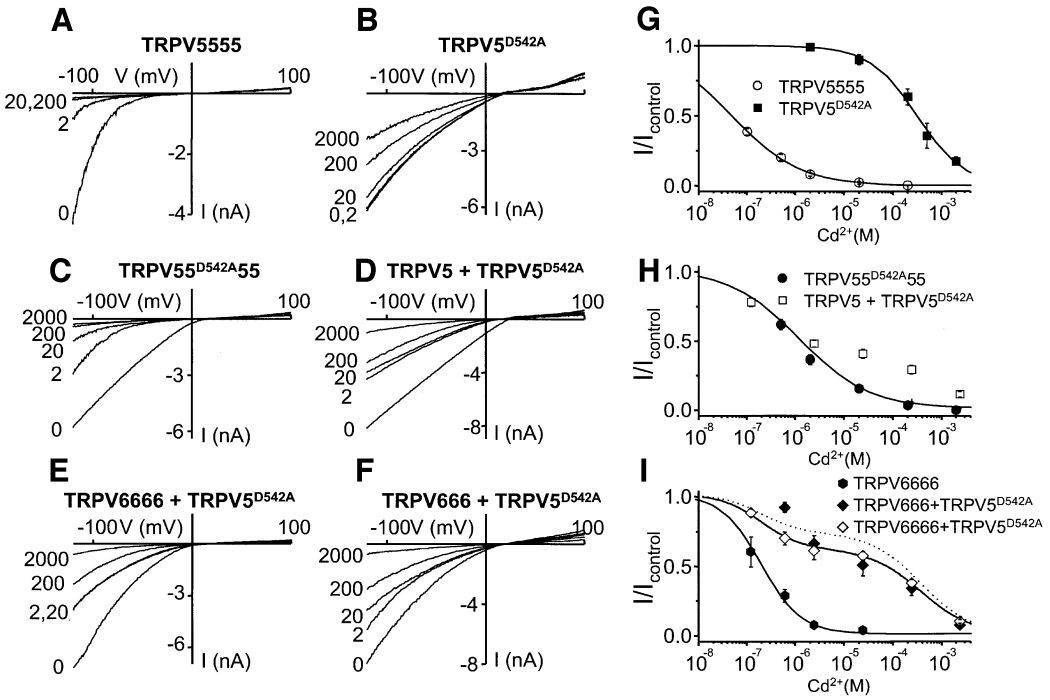

Fig. 6. Cd^{2+} sensitivity of TRPV5, TRPV6 and $TRPV5^{D542A}$ mono- and multimers. (A–F) Current–voltage relationships obtained during voltage ramps in nominally divalent-free extracellular solutions in the absence and presence of 2, 20, 200 and 2000 μM $CdCl_2$ for cells transfected with (**A**) TRPV5555, (**B**) $TRPV5^{D542A}$, (**C**) $TRPV55^{D542A}55$, (**D**) a mixture of TRPV5 and $TRPV5^{D542A}$ in a 3:1 ratio, (**E**) a mixture of TRPV6666 and $TRPV5^{D542A}$ in a 1:1 ratio and (**F**) a mixture of TRPV666 and $TRPV5^{D542A}$ in a 1:1 ratio. (G–I) Dose–response curves for the effect of Cd^{2+} measured at –100 mV. (**G**) Dose–response curves for TRPV5555 and $TRPV5^{D542A}$. From Hill functions fitted to the data (solid curves), we obtained values for K_D and n_{Hill} of 64 nM and 0.78, respectively, for TRPV5555 compared with 313 μM and 0.84 for $TRPV5^{D542A}$. Note that the Cd^{2+} sensitivity of the TRPV5555 concatemer was not significantly different from that of the TRPV5 monomers (K_D = 74 nM, n_{Hill} = 0.81; data not shown). (**H**) Dose–response curves for $TRPV55^{D542A}55$ and the mixture of TRPV5 and $TRPV5^{D542A}$. From a Hill function fitted to the $TRPV55^{D542A}55$ data (solid curve), we obtained values for K_D and n_{Hill} of 1.0 μM and 0.77, respectively. The data for the mixture of TRPV5 and $TRPV5^{D542A}$ were not well fitted by a single Hill function, indicating a population of channels with distinct Cd^{2+} sensitivities. (**I**) Dose–response curves for TRPV6666 and for mixtures of $TRPV5^{D542A}$ with TRPV6666 and TRPV666, respectively. From a Hill function fitted to the TRPV6666 data, values for K_D and n_{Hill} of 163 nM and 1.05, respectively, were obtained. Similar values were obtained for TRPV666 (K_D = 157 nM, n_{Hill} = 0.93) and for the TRPV6 monomer (K_D = 261 nM, n_{Hill} = 1.05). The dose–response curve for the mixture of TRPV6666 and $TRPV5^{D542A}$ was well described by the weighted sum of the Hill functions for TRPV6666 and $TRPV5^{D542A}$ (solid curve). In contrast, the dose–response curve for the mixture of TRPV666 and $TRPV5^{D542A}$ was poorly fitted by the weighted sum of the Hill functions for TRPV6666 and $TRPV5^{D542A}$ (dotted line).

tetrameric stoichiometry of the channel. Wild-type TRPV5 and TRPV6 display voltage-dependent opening of the channel upon hyperpolarization, and deactivation upon depolarization, which is illustrated for TRPV5555 in Figure 7B. The apparent open probability of the channel as a function of voltage, which was determined as the normalized inward current upon stepping to –100 mV from different test potentials, did not differ significantly between TRPV5555, TRPV666, TRPV6666 and monomeric TRPV5 or TRPV6 constructs (Figure 7G; data not shown). This voltage dependence, which depends on intracellular Mg^{2+} (Voets *et al.*, 2001), is abolished in the $TRPV5^{D542A}$ mutant (Figure 7C and G). Interestingly, the effect of this mutation on voltage-dependent gating appears to be dominant, since mutating only a single subunit in a tetrameric TRPV5 construct ($TRPV55^{D542A}55$) resulted in voltage-independent currents (Figure 7D and H). Likewise, co-expression of the TRPV666 construct with $TRPV5^{D542A}$ led to voltage-independent currents, consistent with formation of a TRPV666+$TRPV5^{D542A}$ tetrameric channel (Figure 7E and H). In contrast, voltage-dependent gating was reduced, but not abolished, in cells co-expressing TRPV6666 or TRPV5555 with $TRPV5^{D542A}$, indicating formation of separate voltage-dependent TRPV6666 (or TRPV5555) channels and voltage-independent tetrameric $TRPV5^{D542A}$ channels (Figure 7F and H).

Taken together, these data fully confirm the tetrameric composition of TRPV5/6 channels suggested by the sedimentation and cross-linking experiments. Moreover, they demonstrate that the covalent linking of TRPV5/6 monomers in concatemeric structures has no obvious effect on the properties of the channels and that concatemers are not broken down into individual subunits. Finally, they suggest that heteromultimerization of TRPV5 and TRPV6 subunits produces functional channels.

Functional analysis of concatemeric TRPV5/6 tetramers

To investigate whether different compositions of hetero-tetrameric TRPV5/6 complexes have diverse functional properties, a complete set of TRPV5/6 (hetero)tetrameric channels was generated and subsequently divided into five groups: 5_4 (consisting of TRPV5555), 5_36_1 (consisting of TRPV5556, TRPV5565, TRPV5655, TRPV6555), 5_26_2 (consisting of TRPV5566, TRPV5656, TRPV6655, TRPV6565, TRPV5665, TRPV6556), 5_16_3 (consisting of TRPV6665, TRPV6656, TRPV6566, TRPV5666) and 6_4

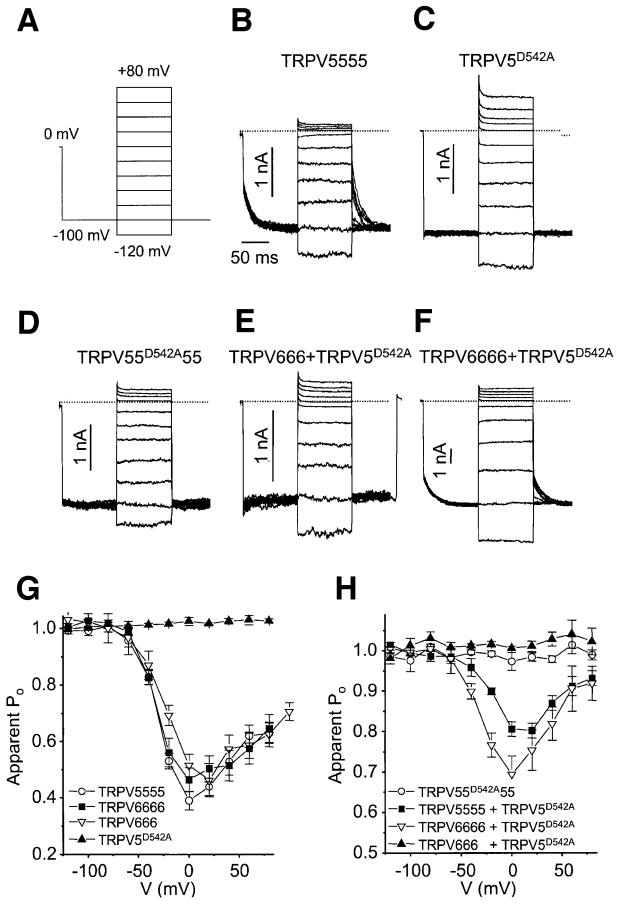

Fig. 7. Dominant-negative effect of the $TRPV5^{D542A}$ mutation on voltage-dependent gating of TRPV5/6 homo- and heterotetramers. (**A**) Voltage protocol. Voltage steps were delivered at a frequency of 0.5 Hz. Note that in these experiments the intracellular solution contained 3 mM $MgCl_2$ (calculated free intracellular Mg^{2+} = 127 μM) instead of the normal 1 mM to accentuate the voltage-dependent behavior of TRPV5/6. (**B**–**F**) Currents measured in divalent-free solution supplemented with 10 mM EDTA from cells expressing the indicated constructs or mixtures of constructs. (**G** and **H**) Voltage dependence of the apparent open probability for the constructs or mixtures of constructs indicated. The apparent open probability was determined as the current immediately upon stepping back to –100 mV normalized to the current at the end of the initial step to –100 mV.

(consisting of TRPV6666). Previous studies have demonstrated that TRPV5 and TRPV6 differ in the kinetics of Ca^{2+}-dependent inactivation, permeability for Ba^{2+} and sensitivity for the potent blocker ruthenium red (Hoenderop *et al*., 2001b). Interestingly, increasing the number of TRPV6 subunits, starting from 5_4, revealed a gradual increase in TRPV6 channel properties, including reduced Ba^{2+} permeability (Figure 8A and C), increased fast Ca^{2+}-dependent inactivation (Figure 8A and D) and reduced inhibition by 1 μM ruthenium red (Figure 8B). Replacing a single TRPV5 subunit by a TRPV6 subunit in a TRPV5 tetramer induced kinetic properties of the TRPV6 channel. The relative position of such a TRPV5 or TRPV6 subunit in a homotetrameric complex, i.e. TRPV5655 or TRPV5565, did not significantly affect the measured kinetics (data not shown). Moreover, using a similar approach to that in Figure 7, we found that the voltage-dependent gating of the different heterotetrameric channels was indistinguishable from that of TRPV5 or TRPV6 homotetrameric channels (data not shown).

Discussion

In the present study, we have combined several independent methods to demonstrate that TRPV5 and TRPV6 are functional as homo- and heterotetrameric Ca^{2+} channels with novel properties. This conclusion is based on the following observations. First, chemical cross-linking experiments revealed protein band shifts from monomeric TRPV5 and TRPV6 to multimeric compositions. Secondly, sucrose gradient centrifugation confirmed that TRPV5 and TRPV6 channel complexes have a molecular weight in line with a tetrameric configuration. Thirdly, co-immunoprecipitations demonstrated that TRPV5 and TRPV6 subunits are physically linked to each other. Fourthly, electrophysiological analyses of concatemeric polypeptides revealed that all (hetero)tetrameric TRPV5/6 channels are functional with differences in transport kinetics.

Post-translational modification of TRPV5 and TRPV6

Our data indicated that both high mannose type glycosylation and complex glycosylation of TRPV5 and TRPV6 occur. Analysis of the primary structure of TRPV5/6 revealed a conserved *N*-glycosylation sequence in the first extracellular loop (Hoenderop *et al*., 2001b). As complex glycosylation is established in the *trans*-Golgi network, the presence of TRPV5/6 in a state of complex glycosylation indicates that the synthesis of TRPV5 and TRPV6 is fully matured and therefore the oocyte expression system is useful for studying the oligomerization state of these channels. N-linked glycosylation could play a role in protein folding since it has been demonstrated that glycosylation is crucial for the stability and assembly of Shaker potassium channels into a multimeric complex (Khanna *et al*., 2001). Given the conserved overall topology of these potassium and TRP channels, it is feasible that glycosylation determines the stability and assembly of TRPV5 and TRPV6.

Co-expression and regulation of TRPV5 and TRPV6

Expression studies using RT–PCR and northern blot analysis of various tissues revealed co-expression of TRPV5 and TRPV6 in the small intestine, kidney, pancreas, testis and prostate (Muller *et al*., 2000a; Peng *et al*., 2000; Hoenderop *et al*., 2001b). The relative expression of these channels could differ between tissues. For instance, mRNA levels of TRPV6 are relatively high in duodenum, whereas TRPV5 is predominantly expressed in kidney (van Cromphaut *et al*., 2001). This study provides the first evidence that TRPV6 is co-expressed with TRPV5 along the apical membrane of renal distal tubular cells. The observed apical co-localization of the TRPV5/6 proteins in kidney cells emphasizes the physiological relevance of the interaction between TRPV5 and TRPV6 in functional tetrameric ion channels.

Channel assembly may be a highly optimized cellular process in which a balance between tetramerization and monomer degradation has physiological significance at the level of channel gene expression ultimately realized at the

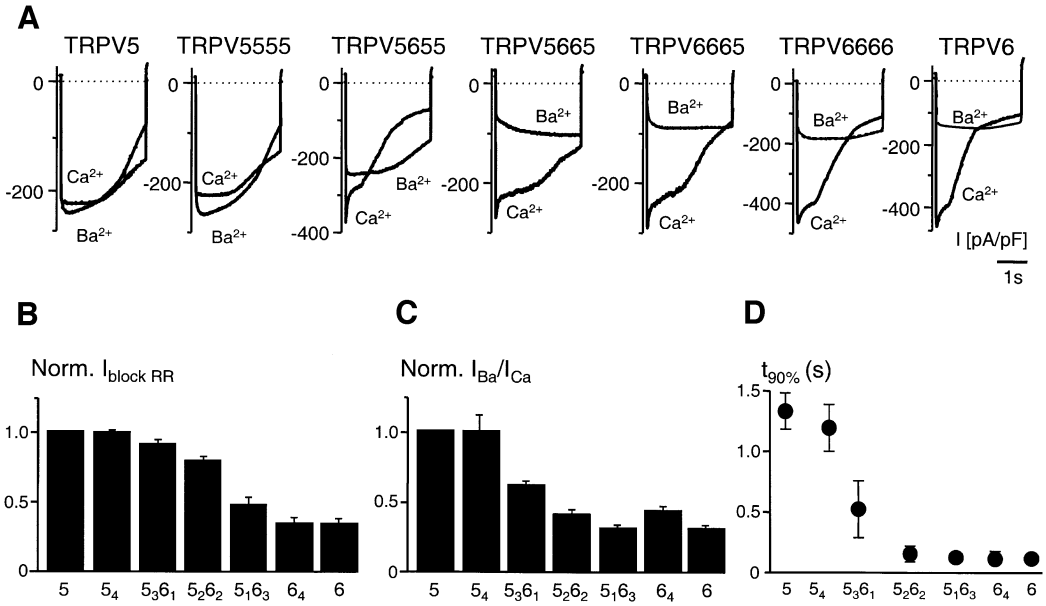

Fig. 8. Expression and analysis of (hetero)tetrameric TRPV5/6 channels in HEK293 cells. (**A**) Currents at hyperpolarizing steps from the +20 mV holding potential to –100 mV. Extracellular Ca^{2+} and Ba^{2+} concentration was 30 mM. Current densities, expressed per unit membrane capacitance, were calculated from the current at –80 mV during the ramp protocols. (**B**) Normalized current block of heterotetrameric proteins by ruthenium red (1 μM). (**C**) Normalized I_{Ba}/I_{Ca} current ratio. (**D**) Inactivation kinetics of heterotetrameric proteins. Fast inactivation was assessed by the time for 10% decay ($t_{90\%}$) of the current, and the slower run down by the time constant of a mono-exponential fit of the current during the last 1.5 s of the step.

cell surface. In this respect, it is important to note that TRPV5 and TRPV6 are tightly controlled by 1,25-dihydroxyvitamin D_3 and dietary Ca^{2+} content (Hoenderop *et al.*, 2001a, 2002a; van Cromphaut *et al.*, 2001; Weber *et al.*, 2001; Wood *et al.*, 2001; Brown *et al.*, 2002). Recently, it was found that TRPV5 expression in kidney is regulated by 17β-estradiol (Van Abel *et al.*, 2002). Taken together, TRPV5 and TRPV6 are controlled by various hormones, and differential regulation of their expression, and consequently their stoichiometry, may be a mechanism for fine tuning the Ca^{2+} transport kinetics in TRPV5/6-expressing tissues.

TRPV5 and TRV6 form heterotetrameric complexes

The first indication that the epithelial Ca^{2+} channel forms multimeric complexes at the plasma membrane came from cross-linking studies using oocyte membranes expressing TRPV5 or TRPV6. In the presence of the chemical cross-linker DTBP, the protein bands clearly shifted to complexes of a larger molecular size, indicating that monomeric subunits are no longer present and that multimeric complexes between channel subunits have been formed. Recently, the oligomeric structure of another TRP member, the vanilloid receptor type 1 (TRPV1), was studied by biochemical cross-linking (Kedei *et al.*, 2001). Their findings suggested the predominant existence of tetramers, in line with our present data for TRPV5/6. In addition, sucrose gradient analysis of TRPV5/6-expressing oocytes revealed that TRPV5 and TRPV6 are sedimented as a complex of ~400 kDa, which is in line with a tetrameric architecture. In the presence of SDS, this complex disintegrated and only monomeric subunits were detected. Finally, the tetrameric structure was investigated in a functional assay, following a similar approach to that previously used to prove the tetrameric stoichiometry of the structurally related Shaker-like potassium channels (Liman *et al.*, 1992) and cyclic nucleotide-gated channels (Liu *et al.*, 1996). Our method made use of the observation that $TRPV5^{D542A}$, a pore mutant of TRPV5, has a >1000-fold reduced Cd^{2+} sensitivity and a dominant-negative effect on the voltage-dependent gating of TRPV5/6. Our results demonstrated that $TRPV5^{D542A}$ can combine with a trimeric TRPV666 construct, but is excluded from tetrameric TRPV6666 or TRPV5555 concatemers, which implies that functional TRPV5/6 channels are indeed tetramers.

Detailed information concerning protein structure and assembly of ion channels containing six transmembrane-spanning domains, including a pore domain between TM 5 and TM 6, is only available for Shaker-like potassium and cyclic nucleotide-gated channels. The clustering of four subunits in six transmembrane domain channels is assumed to create an aqueous pore centered around the 4-fold symmetry axis (Kreusch *et al.*, 1998). We have previously demonstrated that a single aspartic residue in the aqueous pore region of TRPV5 (D542) determines the Ca^{2+} permeation of the channel (Nilius *et al.*, 2001c). The tetrameric architecture of TRPV5/6 elucidated in the present work implies that four aspartates contribute to the selectivity filter for Ca^{2+}, by analogy with the four negatively charged glutamates and/or aspartates that determine the Ca^{2+} selectivity in voltage-gated Ca^{2+} channels (Hess and Tsien, 1984). Although the overall structure of TRPV5/6 is similar to that of voltage-gated Ca^{2+} channels, the mode of subunit assembly appears to be different for TRPV5/6, since four individual TRPV5 and/or TRPV6 subunits have to assemble to form a functional channel, whereas functional voltage-gated Ca^{2+} channels are monomeric proteins containing four homologous internal repeats.

Functional consequences of TRPV5/6 heterotetramerization

Heterotetrameric TRPV5/6 proteins displayed properties that, depending on the subunit configuration, are intermediate between TRPV5 and TRPV6. Replacing TRPV5 by TRPV6 subunits in a TRPV5 tetramer has major effects on Ba^{2+} permeability, Ca^{2+}-dependent inactivation and the block by ruthenium red. In this way, Ca^{2+}-transporting epithelia co-expressing TRPV5 and TRPV6 may be able to generate a pleiotropic set of functional heterotetrameric channels. Variation in the individual subunits of this tetramer (i.e. TRPV5, TRPV6 or post-translational modified subunits) could provide a mechanism for fine tuning the Ca^{2+} transport kinetics in Ca^{2+}-transporting epithelia.

It was recently proposed that TRPV6 exhibits the unique biophysical properties of the Ca^{2+}-release-activated Ca^{2+} channel (CRAC) and comprises all or part of the CRAC pore (Yue *et al*., 2001). These authors also suggested that TRPV5 could account for CRAC in some cells. However, subsequent studies demonstrated that TRPV6 and CRAC have clearly distinct pore properties (Voets *et al*., 2001; Bodding *et al*., 2002). One of the major differences between CRAC and TRPV6 was the voltage-dependent gating, which is prominent in TRPV6 but absent in CRAC, although the possibility that the CRAC pore consists of TRPV6 in combination with additional unknown subunits (e.g. TRPV5) could not be excluded. However, our present results show that all possible TRPV5–TRPV6 heteromultimeric concatemers exhibit voltage-dependent gating.

Conclusions

In the present study, we have demonstrated that the epithelial Ca^{2+} channels TRPV5 and TRPV6 have a tetrameric stoichiometry and can combine with each other to form heteromultimeric channels with novel properties. Thus, the picture obtained from extensive structure–function studies on voltage-gated K^+ channels, namely a membrane protein formed by four subunits in a ring-like structure around a central pore, also seems to apply to TRPV5/6 and probably to all members of the TRPV family.

Materials and methods

Construction of tagged TRPV5/6 proteins

Wild-type rabbit TRPV5 and mouse TRPV6 were tagged with an HA and a Flag tag, respectively. DNA encoding HA or Flag was cloned at the 5′ site of the wild-type constructs. The N-terminally tagged TRPV5/6 fragments were amplified with *Pfu* polymerase (Stratagene, La Jolla, CA) using the forward primer 5′-CAGATCGCGAGCCACCATGTACCCA-TACGACGTGCCAGACTACGCAGGGGCCTGTCCACCCAAGGCA--3′ and the reverse primer 5′-CCCAGGGAGTCCTGGGCCCGG-3′ for TRPV5, and the forward primer 5′-CAGATCGCGAGCCACCATGGA-CTACAAGGATGACGATGACAAGGGGTGGTCCCTGCCCAAGG-AGAAG-3′ and reverse primer: 5′-GGACAAAGGGTGCTCTCCATA-3′) in a PCR with the wild-type TRPV5 and TRPV6 pTLN-constructs as a template. The obtained DNA fragments were digested with *Afl*II for TRPV5 and *Spe*I for TRPV6, and subsequently cloned in pTLN that was digested with *Nru*I and *Afl*II or with *Nru*I and *Spe*I, respectively. G-capped cRNA transcripts were synthesized as described previously (Hoenderop *et al*., 1999b).

Preparation of oocytes

Oocytes were isolated from *X.laevis* and injected with 10 ng of cRNA of HA-TRPV5 and/or wild-type Flag-TRPV6. Two days after injection, membrane lysates were prepared as described previously (Hoenderop *et al*., 1999b). To isolate total membranes, 50–100 oocytes were homogenized in 1 ml of homogenization buffer (HBA) (20 mM Tris–HCl pH 7.4, 5 mM $MgCl_2$, 5 mM NaH_2PO_4, 1 mM EDTA, 80 mM sucrose, 1 mM PMSF, 10 μg/ml leupeptin and 50 μg/ml pepstatin) and centrifuged twice at 3000 *g* for 10 min at 4°C to remove yolk proteins. Subsequently, membranes were isolated by centrifugation at 14 000 *g* for 30 min at 4°C as described previously (Kamsteeg *et al*., 1999).

Immunoblot analysis

Aliquots of proteins in loading buffer were subjected to SDS–PAGE (8% w/v) and subsequently electroblotted onto PVDF membranes. Blots were incubated with 5% (w/v) non-fat dried milk in TBS-T [137 mM NaCl, 0.2% (v/v) Tween-20 and 20 mM Tris pH 7.6]. Immunoblots were incubated overnight at 4°C with the primary antibodies indicated including mouse anti-HA (Roche, Indianapolis, IN), 1:4000, 1% (w/v) milk in TBS-T, mouse anti-Flag (Sigma, St Louis, MO), 1:8000, 5% (w/v) milk in TBS-T, mouse anti-Flag peroxidase coupled (Sigma), 1:2000, 5% (w/v) milk in TBS-T and guinea pig anti-TRPV5 (Hoenderop *et al*., 2000), 1:500, 1% (w/v) milk in TBS-T. Blots were incubated at room temperature with the corresponding secondary antibodies including sheep anti-mouse IgG peroxidase (Sigma), 1:2000 in TBS-T, for 1 h or goat anti-guinea pig IgG peroxidase (Sigma), 1:10 000, for 1 h as described previously (Hoenderop *et al*., 1999a).

Deglycosylation with endoF and endoH

Deglycosylation with endoF and endoH (Biolabs, Beverly, MA) was performed in a volume of 50 μl with cell homogenate isolated from five oocytes resuspended in Laemmli buffer. The endoF reaction was carried out in 40 mM sodium phosphate buffer pH 7.5 with 0.4% (w/v) SDS, 20 mM DTT and 0.8% (v/v) NP-40. After addition of 500 U of endoF, the mixture was incubated at 37°C for 60 min. EndoH treatment was carried out in 40 mM sodium citrate buffer pH 5.5 with an SDS concentration of 0.4% (w/v). After addition of 500 U of endoH, the mixture was incubated at 37°C for 60 min and separated by electrophoresis on an 8% (w/v) SDS gel.

Cross-linking studies

Total membrane preparations of oocytes expressing TRPV5 or TRPV6 were resuspended and incubated for 30 min at 37°C in cross-linking buffer [1% (w/v) sodium desoxycholate, 20 mM HEPES, 5 mM KCl, 130 mM NaCl, 10% (v/v) glycerol, 5 mM EDTA, protease inhibitors, NaOH pH 7.2]. Samples were divided into three equal amounts. Two parts were treated with 2 mM DTBP in cross-linking buffer and incubated for 60 min on ice. Subsequently, cross-linking was terminated by the addition of 100 mM Tris and samples were incubated for 30 min on ice. Samples were incubated in Laemmli buffer for 30 min at 37°C with and without 100 mM DTT. As a control, the third part was not treated with DTBP.

Co-immunoprecipitation

Twenty-microliter equivalents of protein A-coupled agarose beads (Pharmacia, Uppsala, Sweden) were pre-incubated for 16 h (overnight) at 4°C with 2 μl of monoclonal anti-HA antibody (Sigma) in 0.7 ml of IPP500 [500 mM NaCl, 10 mM Tris pH 8.0, 0.1% (v/v) NP-40, 0.1% (v/v) Tween-20, 1 mM PMSF, 10 μg/ml leupeptin, 50 μg/ml pepstatin] and 0.1% (w/v) bovine serum albumin. The beads were washed three times with IPP100 (100 mM NaCl, 10 mM Tris pH 8.0, 0.1% NP-40, 0.1% Tween-20). Isolated total membranes of 15 oocytes expressing HA-TRPV5 or Flag-TRPV6, or co-expressing both, were incubated for 1 h at 37°C in 50 μl of solubilization buffer [20 mM Tris pH 8.0, 10% (v/v) glycerol, 5 mM EDTA, 0.5% (w/v) sodium desoxycholate, 1 mM PMSF, 10 μg/ml leupeptin, 50 μg/ml pepstatin] and centrifuged at 16 000 *g* for 1 h at 4°C to pellet undissolved membranes. The solubilized membranes were diluted with 700 μl of sucrose buffer [100 mM NaCl, 20 mM Tris pH 8.0, 5 mM EDTA, 0.1% (v/v) Triton X-100, 10% (w/v) sucrose, 1 mM PMSF, 10 μg/ml leupeptin, 50 μg/ml pepstatin], added to the washed antibody-bound protein A beads and incubated for 16 h at 4°C. After incubation, the beads were washed three times with IPP100, incubated in 25 μl of Laemmli buffer for 30 min at 37°C and subjected to immunoblotting.

Sedimentation by sucrose gradient centrifugation

Total membranes of 100 oocytes injected with HA-TRPV5 or Flag-TRPV6 were incubated in solubilization buffer [0.5% sodium deoxycholate, 20 mM Tris pH 8.0, 5 mM EDTA, 10% (v/v) glycerol, 1 mM PMSF, 10 μg/ml leupeptin, 50 μg/ml pepstatin] for 1 h at 37°C and

subsequently centrifuged at 100 000 *g* for 1 h at 4°C to pellet undissolved membranes. Samples were supplemented with gradient buffer (20 mM Tris pH 8.0, 5 mM EDTA, 0.1% Triton X-100, 1 mM PMSF, 10 µg/ml leupeptin, 50 µg/ml pepstatin) to 300 µl. Sedimentation by gradient centrifugation was carried out essentially as described previously (Jung *et al*., 1994). Solutions of 10, 15, 20, 25, 30 and 35% sucrose each in gradient buffer were prepared. The dissolved membrane samples were loaded onto the gradient and subjected to 150 000 *g* centrifugation for 16 h at 8°C. Then 200 µl fractions were carefully removed, designated A–R and analyzed by immunoblotting. A mixture of phosphorylase B (97 kDa), yeast alcohol dehydrogenase (150 kDa), catalase (232 kDa) and apoferritin (443 kDa) was used as sedimentation markers. All markers were obtained from Sigma.

Expression of concatemeric cDNA constructs

Concatemeric constructs were produced by linking the coding sequences of TRPV5 and TRPV6 subunits in a head-to-tail fashion. Two types of TRPV5/6 constructs were constructed: a 3′-modified construct in which the stop codon was mutated to contain a unique *Pme*I (GTTTAAAC) restriction site followed by a unique *Bsi*WI (CGTACG) restriction site in the 3′ non coding region, and a 5′–3′-modified construct containing the 3′ construct modifications described above. In addition, a linker of eight glutamines was inserted as an inter-subunit bridge in front of the 5′-ATG codon containing a unique *Eco*RV restriction site in the first 5′ glutamine codon (Firsov *et al*., 1998). To use the applied strategy, the internal *Eco*RV restriction site in TRPV5 (nucleotide position 1190) has been mutated without affecting the amino acid sequence. Multimeric constructs were obtained by digestion of the 5′–3′-modified construct with *Eco*RV and *Bsi*WI, and insertion of the digestion product into the 3′-modified construct digested with *Pme*I and *Bsi*WI. By applying this strategy, combinations of concatemeric proteins were constructed including TRPV5555, TRPV6666, TRPV5566, TRPV6655, TRPV6565, TRPV5656, TRPV5665, TRPV6556, TRPV5556, TRPV5565, TRPV5655, TRPV6555, TRPV6665, TRPV6656, TRPV6566, TRPV5666, TRPV666 and TRPV55^{D542A}55. Finally, a short linker containing a 5′ blunt site, a stop codon in the middle and a 3′ *Bsi*WI site was inserted in the concatemeric transcripts mentioned above by digesting the cDNA with *Pme*I and *Bsi*WI. All the DNA constructs obtained were transfected into HEK293 cells as described previously (Vennekens *et al*., 2000).

Electrophysiology

Patch–clamp experiments were performed in the tight-seal whole-cell configuration, using an EPC-9 patch–clamp amplifier (HEKA Elektronik, Lambrecht, Germany). Patch pipettes had DC resistances of 2–4 MΩ when filled with intracellular solution. Series resistances were between 3 and 10 MΩ, and were compensated for 60–80%. The internal (pipette) solution contained 20 mM CsCl, 100 mM Cs aspartate, 1 mM $MgCl_2$, 10 mM BAPTA, 4 mM Na_2ATP and 10 mM HEPES–CsOH pH 7.2. The pipette solution used for the experiments shown in Figure 7 contained 3 mM rather than 1 mM $MgCl_2$. The divalent-free extracellular solution contained 150 mM NaCl, 10 mM EDTA and 10 mM HEPES–NaOH pH 7.4. The solutions used to test for Ca^{2+}- or Ba^{2+}-dependent inactivation contained 150 mM NMDG, 30 mM $CaCl_2$ or $BaCl_2$ and 10 mM HEPES, titrated to pH 7.4 with HCl. EDTA was omitted in the nominally divalent-free solution. All experiments were performed at room temperature (20–22°C).

Immunohistochemistry

Immunohistochemistry was performed as described previously (Hoenderop *et al*., 2000). Briefly, mouse kidney sections were incubated for 16 h at 4°C with affinity-purified guinea pig antiserum against TRPV5 (1:100) or rabbit antiserum against TRPV6 (1:100). The TRPV5 antibody has been extensively characterized previously (Hoenderop *et al*., 2001a). Antiserum against TRPV6 was obtained by immunization of rabbits with synthetic peptide coupled to keyhole limpet haemocyanin representing the last 15 amino acids of the C-tail of mouse TRPV6 (NH_2-INRGLEDGEGWEYQI-COOH) and affinity purified. To visualize TRPV5 and TRPV6, a goat anti-guinea pig Alexa 488-conjugated antibody (1:300) or a goat anti-rabbit Alexa 488-conjugated antibody (1:300) (Molecular Probes, Eugene, OR) was used. All negative controls, including sections incubated with either pre-immune serum or pre-absorbed antiserum for 1 h with 10 µg/ml peptide or solely with conjugated secondary antibodies, were devoid of any staining.

Statistical analysis

Data analysis and display was performed using Microcal Origin software version 7.0 (OriginLab Corporation). Unless noted otherwise, averaged data are shown as mean ± SEM from at least four cells. Dose–response curves were fitted using a Hill function of the form

$$\frac{I}{I_{\text{control}}} = \frac{1}{1 + \left(\frac{C}{K_D}\right)^{n_{\text{Hill}}}}$$

where C is the concentration of blocker, K_D is the concentration for half-maximal inhibition and n_{Hill} is the Hill coefficient. When indicated, dose–response curves were fitted by the weighted sum of two Hill curves:

$$\frac{I}{I_{\text{control}}} = \frac{a}{1 + \left(\frac{C}{K_{D1}}\right)^{n_{\text{Hill1}}}} + \frac{1-a}{1 + \left(\frac{C}{K_{D2}}\right)^{n_{\text{Hill2}}}}$$

where a is a weighting factor.

Acknowledgements

This work was supported by the Dutch Organization of Scientific Research (Zon-Mw 016.006.001, Zon-Mw 902.18.298, NWO-ALW 810.38.004) and in part by the Belgian Federal Government, the Flemish Government and the Onderzoeksraad KU Leuven (GOA 99/07, F.W.O. G.0237.95, F.W.O. G.0214.99, F.W.O. G.0136.00, F.W.O. 0172.03) and a grant from the Alphonse and Jean Forton-Koning Boudewijn Stichting R7115 B0. T.V. is a postdoctoral fellow of the Fund for Scientific Research–Flanders (F.W.O.–Vlaanderen, Belgium). The authors would like to thank Dr C.H.van Os and Dr P.M.T.Deen for critical reading of the manuscript and helpful comments, and A.Janssen for expert technical assistance.

References

Bahner,M., Sander,P., Paulsen,R. and Huber,A. (2000) The visual G protein of fly photoreceptors interacts with the PDZ domain assembled INAD signaling complex via direct binding of activated Gα^q to phospholipase cβ. *J. Biol. Chem.*, **275**, 2901–2904.

Bodding,M., Wissenbach,U. and Flockerzi,V. (2002) The recombinant human TRPV6 channel functions as Ca^{2+} sensor in human embryonic kidney and rat basophilic leukemia cells. *J. Biol. Chem.*, **277**, 36656–36664.

Brown,A.J., Finch,J. and Slatopolsky,E. (2002) Differential effects of 19-nor-1,25-dihydroxyvitamin D_2 and 1,25-dihydroxyvitamin D_3 on intestinal calcium and phosphate transport. *J. Lab. Clin. Med.*, **139**, 279–284.

Clapham,D.E., Runnels,L.W. and Strubing,C. (2001) The TRP ion channel family. *Nat. Rev. Neurosci.*, **2**, 387–396.

Firsov,D., Gautschi,I., Merillat,A.M., Rossier,B.C. and Schild,L. (1998) The heterotetrameric architecture of the epithelial sodium channel (ENaC). *EMBO J.*, **17**, 344–352.

Hess,P. and Tsien,R.W. (1984) Mechanism of ion permeation through calcium channels. *Nature*, **309**, 453–456.

Hoenderop,J.G., Vaandrager,A.B., Dijkink,L., Smolenski,A., Gambaryan,S., Lohmann,S.M., de Jonge,H.R., Willems,P.H. and Bindels,R.J. (1999a) Atrial natriuretic peptide-stimulated Ca^{2+} reabsorption in rabbit kidney requires membrane-targeted, cGMP-dependent protein kinase type II. *Proc. Natl Acad. Sci. USA*, **96**, 6084–6089.

Hoenderop,J.G., van der Kemp,A.W., Hartog,A., van de Graaf,S.F., van Os,C.H., Willems,P.H. and Bindels,R.J. (1999b) Molecular identification of the apical Ca^{2+} channel in 1,25-dihydroxyvitamin D_3-responsive epithelia. *J. Biol. Chem.*, **274**, 8375–8378.

Hoenderop,J.G., Hartog,A., Stuiver,M., Doucet,A., Willems,P.H. and Bindels,R.J. (2000) Localization of the epithelial Ca^{2+} channel in rabbit kidney and intestine. *J. Am. Soc. Nephrol.*, **11**, 1171–1178.

Hoenderop,J.G. *et al*. (2001a) Calcitriol controls the epithelial calcium channel in kidney. *J. Am. Soc. Nephrol.*, **12**, 1342–1349.

Hoenderop,J.G., Vennekens,R., Muller,D., Prenen,J., Droogmans,G., Bindels,R.J. and Nilius,B. (2001b) Function and expression of the epithelial Ca^{2+} channel family: comparison of the mammalian epithelial Ca^{2+} channel 1 and 2. *J. Physiol.*, **537**, 747–761.

Hoenderop,J.G., Dardenne,O., Van Abel,M., Van Der Kemp,A.W., Van Os,C.H., St -Arnaud,R. and Bindels,R.J. (2002a) Modulation of renal Ca^{2+} transport protein genes by dietary Ca^{2+} and 1,25-dihydroxyvitamin D_3 in 25-hydroxyvitamin D_3-1α-hydroxylase knockout mice. *FASEB J.*, **16**, 1398–1406.

Hoenderop,J.G., Nilius,B. and Bindels,R.J. (2002b) Molecular mechanism of active Ca^{2+} reabsorption in the distal nephron. *Annu. Rev. Physiol.*, **64**, 529–549.

Hofmann,T., Schaefer,M., Schultz,G. and Gudermann,T. (2002) Subunit composition of mammalian transient receptor potential channels in living cells. *Proc. Natl Acad. Sci. USA*, **99**, 7461–7466.

Jung,J.S., Preston,G.M., Smith,B.L., Guggino,W.B. and Agre,P. (1994) Molecular structure of the water channel through aquaporin CHIP. The hourglass model. *J. Biol. Chem.*, **269**, 14648–14654.

Kamsteeg,E.J., Wormhoudt,T.A., Rijss,J.P., van Os,C.H. and Deen,P.M. (1999) An impaired routing of wild-type aquaporin-2 after tetramerization with an aquaporin-2 mutant explains dominant nephrogenic diabetes insipidus. *EMBO J.*, **18**, 2394–2400.

Kedei,N., Szabo,T., Lile,J.D., Treanor,J.J., Olah,Z., Iadarola,M.J. and Blumberg,P.M. (2001) Analysis of the native quaternary structure of vanilloid receptor 1. *J. Biol. Chem.*, **276**, 28613–28619.

Khanna,R., Myers,M.P., Laine,M. and Papazian,D.M. (2001) Glycosylation increases potassium channel stability and surface expression in mammalian cells. *J. Biol. Chem.*, **276**, 34028–34034.

Kreusch,A., Pfaffinger,P.J., Stevens,C.F. and Choe,S. (1998) Crystal structure of the tetramerization domain of the Shaker potassium channel. *Nature*, **392**, 945–948.

Li,H.S. and Montell,C. (2000) TRP and the PDZ protein, INAD, form the core complex required for retention of the signalplex in *Drosophila* photoreceptor cells. *J. Cell Biol.*, **150**, 1411–1422.

Liman,E.R., Tytgat,J. and Hess,P. (1992) Subunit stoichiometry of a mammalian K^+ channel determined by construction of multimeric cDNAs. *Neuron*, **9**, 861–871.

Lintschinger,B., Balzer-Geldsetzer,M., Baskaran,T., Graier,W.F., Romanin,C., Zhu,M.X. and Groschner,K. (2000) Coassembly of Trp1 and Trp3 proteins generates diacylglycerol- and Ca^{2+}-sensitive cation channels. *J. Biol. Chem.*, **275**, 27799–27805.

Liu,D.T., Tibbs,G.R. and Siegelbaum,S.A. (1996) Subunit stoichiometry of cyclic nucleotide-gated channels and effects of subunit order on channel function. *Neuron*, **16**, 983–990.

Loffing,J., Loffing-Cueni,D., Valderrabano,V., Klausli,L., Hebert,S.C., Rossier,B.C., Hoenderop,J.G., Bindels,R.J. and Kaissling,B. (2001) Distribution of transcellular calcium and sodium transport pathways along mouse distal nephron. *Am. J. Physiol. Renal Physiol.*, **281**, F1021–F1027.

Montell,C. *et al*. (2002) A unified nomenclature for the superfamily of TRP cation channels. *Mol. Cell*, **9**, 229–231.

Muller,D. *et al*. (2000a) Molecular cloning, tissue distribution and chromosomal mapping of the human epithelial Ca^{2+} channel (ECAC1). *Genomics*, **67**, 48–53.

Muller,D., Hoenderop,J.G., Merkx,G.F., van Os,C.H. and Bindels,R.J. (2000b) Gene structure and chromosomal mapping of human epithelial calcium channel. *Biochem. Biophys. Res. Commun.*, **275**, 47–52.

Nilius,B., Prenen,J., Vennekens,R., Hoenderop,J.G., Bindels,R.J. and Droogmans,G. (2001a) Modulation of the epithelial calcium channel, ECaC, by intracellular Ca^{2+}. *Cell Calcium*, **29**, 417–428.

Nilius,B., Prenen,J., Vennekens,R., Hoenderop,J.G., Bindels,R.J. and Droogmans,G. (2001b) Pharmacological modulation of monovalent cation currents through the epithelial Ca^{2+} channel ECaC1. *Br. J. Pharmacol.*, **134**, 453–462.

Nilius,B., Vennekens,R., Prenen,J., Hoenderop,J.G., Droogmans,G. and Bindels,R.J. (2001c) The single pore residue D542 determines Ca^{2+} permeation and Mg^{2+} block of the epithelial Ca^{2+} channel. *J. Biol. Chem.*, **276**, 1020–1025.

Peng,J.B., Chen,X.Z., Berger,U.V., Vassilev,P.M., Tsukaguchi,H., Brown,E.M. and Hediger,M.A. (1999) Molecular cloning and characterization of a channel-like transporter mediating intestinal calcium absorption. *J. Biol. Chem.*, **274**, 22739–22746.

Peng,J.B., Chen,X.Z., Berger,U.V., Weremowicz,S., Morton,C.C., Vassilev,P.M., Brown,E.M. and Hediger,M.A. (2000) Human calcium transport protein CaT1. *Biochem. Biophys. Res. Commun.*, **278**, 326–332.

Strubing,C., Krapivinsky,G., Krapivinsky,L. and Clapham,D.E. (2001) TRPC1 and TRPC5 form a novel cation channel in mammalian brain. *Neuron*, **29**, 645–655.

Van Abel,M., Hoenderop,J.G., Dardenne,O., St Arnaud,R., Van Os,C.H., Van Leeuwen,H.J. and Bindels,R.J. (2002) 1,25-dihydroxyvitamin D_3-independent stimulatory effect of estrogen on the expression of ECaC1 in the kidney. *J. Am. Soc. Nephrol.*, **13**, 2102–2109.

van Cromphaut,S. *et al*. (2001) Active duodenal calcium absorption in vitamin D receptor-knock out mice: functional and molecular aspects. *Proc. Natl Acad. Sci. USA*, **98**, 13324–13329.

Vennekens,R., Hoenderop,J.G., Prenen,J., Stuiver,M., Willems,P.H., Droogmans,G., Nilius,B. and Bindels,R.J. (2000) Permeation and gating properties of the novel epithelial Ca^{2+} channel. *J. Biol. Chem.*, **275**, 3963–3969.

Vennekens,R., Voets,T., Bindels,R.J., Droogmans,G. and Nilius,B. (2002) Current understanding of mammalian TRP homologues. *Cell Calcium*, **31**, 253–264.

Voets,T. *et al*. (2001) CaT1 and the calcium release-activated calcium channel manifest distinct pore properties. *J. Biol. Chem.*, **276**, 47767–47770.

Weber,K., Erben,R.G., Rump,A. and Adamski,J. (2001) Gene structure and regulation of the murine epithelial calcium channels ECaC1 and 2. *Biochem. Biophys. Res. Commun.*, **289**, 1287–1294.

Wood,R.J., Tchack,L. and Taparia,S. (2001) 1,25-dihydroxyvitamin D_3 increases the expression of the CaT1 epithelial calcium channel in the Caco-2 human intestinal cell line. *BMC Physiol.*, **1**, 11.

Yue,L., Peng,J.B., Hediger,M.A. and Clapham,D.E. (2001) CaT1 manifests the pore properties of the calcium-release-activated calcium channel. *Nature*, **410**, 705–709.

Received August 28, 2002; revised November 25, 2002; accepted December 16, 2002